

## Edge-state transport in graphene $p$ - $n$ junctions in the quantum Hall regime

Nikolai N. Klimov,<sup>1,2,\*</sup> Son T. Le,<sup>1,3,\*</sup> J. Yan,<sup>3</sup> Pratik Agnihotri,<sup>4</sup> Everett Comfort,<sup>4</sup> Ji Ung Lee,<sup>4</sup> David B. Newell,<sup>1</sup> and Curt A. Richter<sup>1</sup>

<sup>1</sup>Physical Measurement Laboratory, NIST, Gaithersburg, Maryland 20899, USA

<sup>2</sup>Joint Quantum Institute, University of Maryland, College Park, Maryland 20742, USA

<sup>3</sup>Department of Physics, University of Massachusetts, Amherst, Massachusetts 01003, USA

<sup>4</sup>College of Nanoscale Science and Engineering, SUNY Polytechnic Institute, Albany, New York 12203, USA

(Received 27 February 2015; published 7 December 2015)

We experimentally investigate charge carrier transport in a graphene  $p$ - $n$  junction device by using independent  $p$ -type and  $n$ -type electrostatic gating which allow full characterization of the junction interface in the quantum Hall regime covering a wide range of filling factors [ $-10 \leq (\nu_1, \nu_2) \leq 10$ ]. Recent charge transport measurements across a graphene  $p$ - $n$  junction in this quantized regime presume that equilibration of all of the Landauer-Büttiker edge states occurs across the  $p$ - $n$  junction interface. Here we show that, in our devices, only the edge state associated with the lowest Landau level fully equilibrate across the  $p$ - $n$  junction, while none of the other edge states equilibrate to transmit current across the junction.

DOI: [10.1103/PhysRevB.92.241301](https://doi.org/10.1103/PhysRevB.92.241301)

PACS number(s): 73.43.Qt, 72.80.Vp, 73.40.-c, 85.35.-p

Graphene, a single layer honeycomb lattice of carbon atoms, is a fascinating material platform to study fundamental solid state physics, with potential post-silicon electronic applications [1]. Realizing and understanding the graphene  $pn$  junction ( $pnJ$ ), with its marked difference from conventional semiconductor  $pnJs$ , is important as it is a promising building block for future graphene electronics [2]. Several interesting transport phenomena are predicted for graphene  $pnJs$  owing to the massless Dirac property of carriers that includes Klein tunneling [3], Veselago lensing [4], and scalable quantum resistance standards [5].

At sufficiently large magnetic fields, graphene exhibits an anomalous quantum Hall effect with quantized Hall resistance values of  $[1/(4n+2)]h/e^2$  with integer number  $n$  and vanishing longitudinal resistance [6–8]. For a graphene  $pnJ$  in the quantum Hall regime, the longitudinal resistances are quantized with nonzero values which depend on the equilibration of the Landauer-Büttiker edge states that arise from the Landau levels (LLs) at the  $pnJ$  interface [9–11]. The nature of the scattering between LLs is a topic of intense experimental and theoretical research over the years [12–15]. However, there is a lack of understanding of a detailed equilibration mechanism and how it depends on device properties. Previous experimental reports [5,9,10,15] have investigated LLs scattering at a graphene  $pnJ$  within a limited range of filling factors where the resulting data can be explained assuming complete equilibration of the edge states. Even in this limited range, it was speculated that slight deviations from full equilibration were an indication of incomplete mode mixing [9].

In this Rapid Communication we report a magnetotransport investigation of a fully symmetric graphene quantum Hall-bar device with a  $pnJ$  formed by using two independent electrostatic back gates that allow the formation of  $p$ - $n$ ,  $p$ - $p$ , or  $n$ - $n$  junctions ( $pnJ$ ,  $ppJ$ ,  $nnJ$ ) over a much wider range of filling factors than have been previously reported. This device geometry allows us to explore thoroughly the edge-state

transport across the junction interface and to determine the range of quantized resistance values that can be obtained, thus providing insight into the nature of edge state equilibration and the subsequent current transport across the graphene  $pnJ$ .

The device was fabricated (see the Supplemental Material [16]) using a specially prepared  $\text{SiO}_2/\text{Si}$  substrate that contains a pair of doped polysilicon gates buried in the  $\text{SiO}_2$  layer 140 nm from the air- $\text{SiO}_2$  interface with a narrow 150 nm gap between the gates (Fig. 1, top left). Chemical-mechanical planarization of the substrate achieves an atomically smooth dielectric surface [17]. A precision technique [18] was used to transfer a single layer exfoliated graphene flake [6] onto the substrate. The graphene flake was then patterned into a Hall bar geometry where the region above the left (right) local gate, G1 (G2) is referred to as region 1 (2) (Fig. 1, top right).

Independent voltages applied to the two polysilicon gates,  $V_{G1}$  and  $V_{G2}$ , allow independent tuning of both carrier type and concentration in the two parts of the graphene conduction channel. We initially measured the four-terminal longitudinal resistance  $R_{14,23}$  [19], with a uniform carrier concentration in the channel ( $V_{G1} = V_{G2}$ ; see [16] for measurement details). As shown in curve (i) of Fig. 2(a), standard longitudinal resistivity behavior is exhibited in the quantum Hall regime with zero resistance values at filling factors  $\nu = (4n+2)$ ,  $n = 0, \pm 1, \pm 2, \dots$ . The charge neutrality point (CNP) is very close to zero gate voltage (CNP =  $-0.4$  V) indicative of high quality, very low intrinsically doped graphene. The Hall mobility of the device measured at low magnetic fields ( $|B| < 3$  T) and at  $T = 0.35$  K was  $\approx 7000$   $\text{cm}^2/\text{Vs}$  as determined at a carrier density of  $n \approx 10^{12}$   $\text{cm}^{-2}$ .

To study the edge-state transport at the  $pnJ$  in the quantum Hall regime, we explored the resistance across the junction as a function of local doping in the conducting channel. When a strong perpendicular magnetic field is applied to the device, holes and electrons in the  $p$  and  $n$  regions of the device condense into quantum Hall states. Bulk electrons and holes are strongly localized by the magnetic field, while transport properties are governed by the formation of chiral LL edge-state channels circulating along the boundary and the  $pnJ$  interface in the opposite direction for  $p$  and  $n$  regions. In

\*These authors contributed equally.

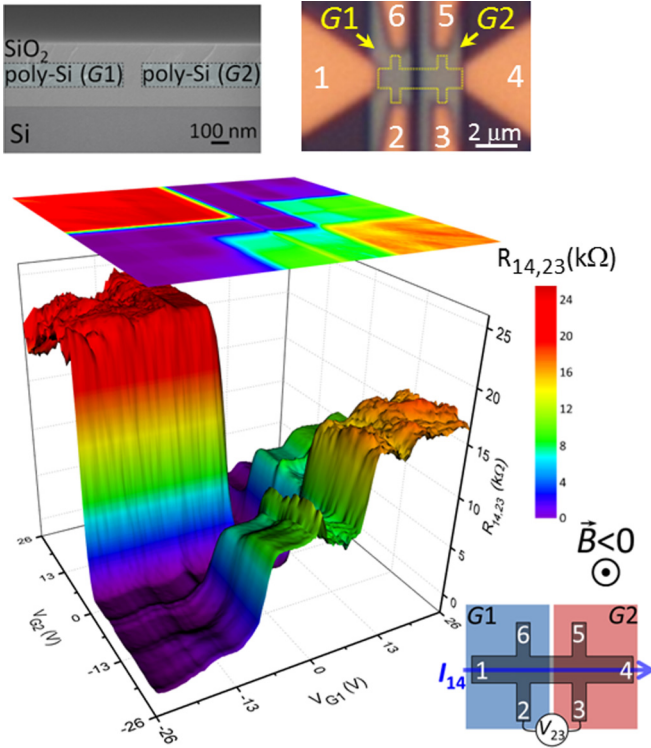


FIG. 1. (Color online) 3D map of longitudinal resistance  $R_{14,23}$  measured at  $T = 0.35$  K and  $B = -14$  T across the junction as a function of local gate voltages  $V_{G1}$  and  $V_{G2}$ . Bottom right: Device schematic with measurement configuration. Top left: SEM image of the substrate's cross section with buried polysilicon gates in  $\text{SiO}_2$ . Top right: Optical image of graphene  $pnJ$  device in a Hall-bar geometry with metal contacts. Graphene Hall bar outlined in yellow.

the quantum Hall regime,  $\nu_1, \nu_2$  are the filling factors in each region (for graphene  $\nu_1, \nu_2 = \pm 2, \pm 6, \pm 10, \dots$ ). Figure 1 shows a 3D map of the measured longitudinal resistance  $R_{14,23}$  across the  $pnJ$  at  $B = -14$  T as a function of  $V_{G1}$  and  $V_{G2}$ . The resistance map reveals a complex picture of quantum Hall plateaus in fractions of  $h/e^2$ . Figure 2(b) is the 2D projection of Fig. 1 with the numbers in each block corresponding to  $h/e^2$  resistance plateau values. For example, the upper-left quadrant of the 2D map ( $pnJ$ :  $V_{G1} < 0$  and  $V_{G2} > 0$ ) is fully occupied with a  $1h/e^2$  plateau, while other areas of the resistance map show plateaus of  $1/15, 1/3, 2/5$ , and  $2/3$  which are located symmetrically about the  $V_{G1} = -V_{G2}$  line.

$$R_{14,23}(h/e^2) = \begin{cases} |1/\nu_1| + |1/\nu_2|, & p\text{-type region, } n\text{-type region 2,} \\ 0, & n\text{-type region, } p\text{-type region 2.} \end{cases} \quad (1c)$$

The upper-left and lower-right quadrants in Fig. 2(c) are modeled resistance values based on Eq. (1c). It is clear that the full equilibration model fails to explain all the measured  $R_{14,23}$  resistance plateaus [bipolar regimes in Fig. 2(b)].

We have developed a model in analogy to the behavior of traditional two-dimensional electron systems in GaAs/AlGaAs heterostructure devices where it was observed that not all LLs fully equilibrate in the quantum Hall regime [22,23]. In our

Junctions at the same polarity ( $pp+$  and  $nn+$ ) correspond to the upper-right ( $nnJ$ :  $V_{G1} > 0$  and  $V_{G2} > 0$ ) and lower-left ( $ppJ$ :  $V_{G1} < 0$  and  $V_{G2} < 0$ ) quadrants of the  $R_{14,23}$  resistance map in Fig. 2(b). For these cases the mechanism of quantum Hall plateau formation can be explained by using the Landauer-Büttiker edge-state formalism [20] with no further assumptions regarding equilibration or nonequilibration of the edge states at the junction. The corresponding edge-state schematic is shown in Fig. 3(a). The edge states that can be accommodated in the lower carrier density region circulate around the entirety of the device's channel including both regions 1 and 2 [black lines in Fig. 3(a)]. Additional edge states arise in the higher carrier concentration region that do not cross the junction interface and circulate only in the region of higher filling factor [red lines in Fig. 3(a)] [15,20,21]. The number of such edge states is equal to  $\nu' = |\nu_1 - \nu_2|$ . Under these conditions, the same equations are obtained for the longitudinal resistance quantum plateaus independent of the equilibration or lack of it between the edge states, and are calculated as follows.

For a unipolar  $ppJ$ ,  $p$  type in both regions 1 and 2:

$$R_{14,23}(h/e^2) = \begin{cases} 0, & |\nu_1| > |\nu_2|, \\ |\nu_1 - \nu_2|/|\nu_1\nu_2|, & |\nu_1| < |\nu_2|. \end{cases} \quad (1a)$$

For a unipolar  $nnJ$ ,  $n$  type in both regions 1 and 2:

$$R_{14,23}(h/e^2) = \begin{cases} |\nu_1 - \nu_2|/|\nu_1\nu_2|, & |\nu_1| > |\nu_2|, \\ 0, & |\nu_1| < |\nu_2|. \end{cases} \quad (1b)$$

The calculated resistance plateaus [Eqs. (1a) and (1b)] in the unipolar regime are shown in upper-right ( $nnJ$  regime) and lower-left ( $ppJ$  regime) quadrants in Figs. 2(c) and 2(d) fully matching the corresponding quadrants of measured  $R_{14,23}$  in Fig. 2(b).

In the case of a bipolar ( $p-n$ ) regime, represented by upper-left and lower-right quadrants of the map in Fig. 2(b), the edge states in the  $p$  and  $n$  regions circulate in opposite directions. Based on a widely accepted model, assuming a full equilibration of countercirculating edge states at the  $pnJ$  interface [10,15,21] [see Fig. 3(b) for edge-state transport schematics] the longitudinal  $R_{14,23}$  resistance plateaus are calculated as follows:

“lowest LL equilibrated” model we assume only the lowest LL's edge states equilibrate at the  $pnJ$ , while the higher LL's edge states propagate along the junction without equilibration or interacting, and contribute no current across the  $pnJ$ . This assumption is supported by numerical simulations in [12,13]. Qualitatively, the higher LL's edge states are energetically separated from the lowest LL and spatially separated from both the lowest LL edge states and the  $pnJ$  interface. Thus,

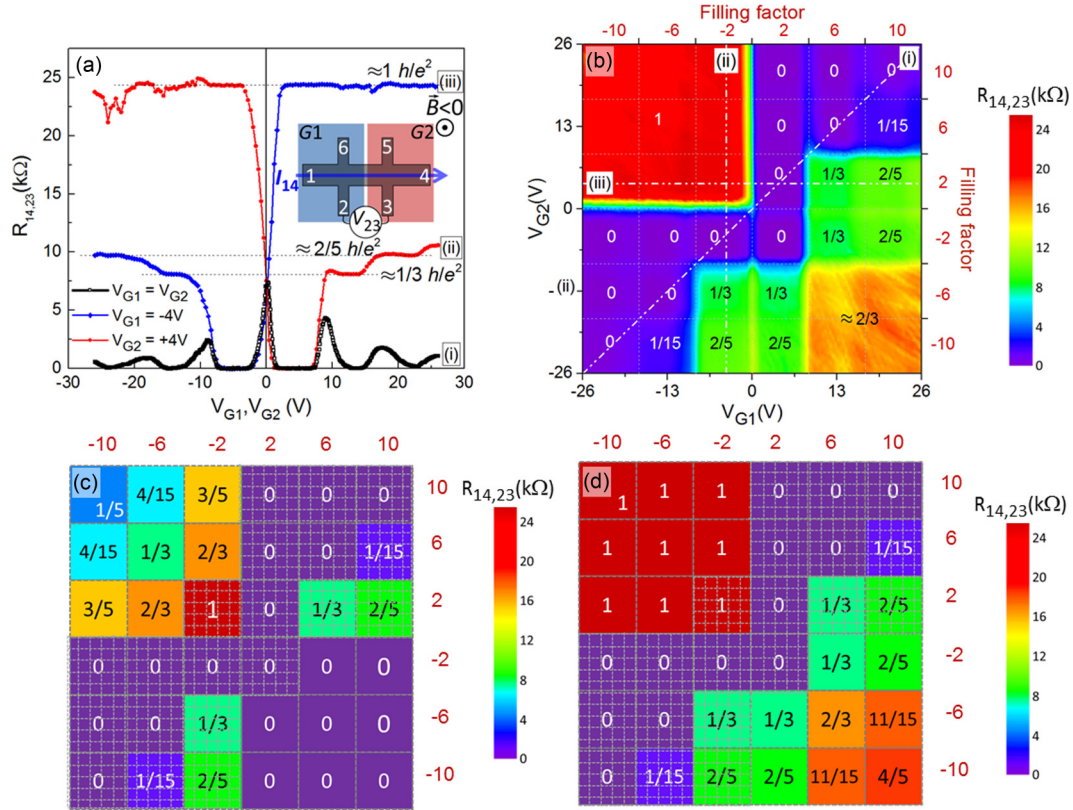


FIG. 2. (Color online) (a) Longitudinal resistance  $R_{14,23}$  measured at  $T = 0.35$  K and  $B = -14$  T as a function of local gate voltages  $V_{G1}$  and  $V_{G2}$ ; (i)  $V_{G1} = V_{G2}$ , (ii)  $V_{G1} = -4$  V, and (iii)  $V_{G2} = +4$  V. Inset shows corresponding measurement configuration. (b) 2D projection of data in Fig. 1 as a function of  $(V_{G1}, V_{G2})$  and filling factors  $(\nu_1, \nu_2)$ . The dash-dotted lines correspond to (i), (ii), and (iii) curves in (a). (c) and (d) Calculated 2D resistance map of  $R_{14,23}$  as a function of filling factors  $(\nu_1, \nu_2)$  assuming (c) full equilibration and (d) only lowest Landau level edge state equilibrated across the junction. The white hashed regions in (c) and (d) are identical and are the regions of previous investigations [5,10,15]. Numbers inside the maps are plateau resistance values in units of  $h/e^2$ .

the lowest LL edge states are expected to have the highest probability to equilibrate and pass current across the junction. In the corresponding schematic of the transport model shown in Fig. 3(c),  $\nu_1'$  and  $\nu_2'$  are the number of edge states in regions 1 and 2 that do not equilibrate across the junction. For  $\nu_1'$  and

$\nu_2'$  we have the following relations:  $\nu_1' = |\nu_1| - 2$ ,  $\nu_2' = |\nu_2| - 2$ , where 2 is the number of edge states of the lowest LL. By using the Landauer-Büttiker formalism with this lowest LL equilibrated assumption, the longitudinal  $R_{14,23}$  resistance is calculated as follows:

$$R_{14,23}(h/e^2) = \begin{cases} 1/(|\nu_1| - \nu_1') + 1/(|\nu_2| - \nu_2') = 1, & p\text{-type region 1, } n\text{-type region 2,} \\ \nu_1'/|\nu_1|(|\nu_1| - \nu_1') + \nu_2'/|\nu_2|(|\nu_2| - \nu_2'), & n\text{-type region 1, } p\text{-type region 2.} \end{cases} \quad (2)$$

The  $R_{14,23}$  resistance map predicted by Eqs. (1a), (1b), and (2) is shown in Fig. 2(d). Similar to the case of the same polarity, the resistance predicted for the  $(2, -2)$  and  $(-2, 2)$  are the same independent of equilibration; however, a dramatic difference is observed for the rest of the bipolar regions in the upper left and lower right of Fig. 2(d). The new model agrees remarkably well with the experimental data [Fig. 2(b)] and accurately describes the quantized resistance values at each  $p$ - and  $n$ -filling factor combination. In other previously reported results [5,10,15], limited filling factors were investigated, as shown in the white hashed regions in Figs. 2(c) and 2(d), where

there is no distinction between full and lowest LL equilibration. Our device geometry enables us to probe well into the bipolar regime where we observe lowest LL equilibration only.

Full equilibration was reported for a two terminal graphene  $pnJ$  device in Williams *et al.* [9], in particular at filling factor  $(6, -2)$  where equilibration can be resolved, although they also reported evidence of incomplete mode mixing at other filling factors. When our device is compared to that of [9], the LL energy spacings, the length of the edge states along the  $pnJ$  interface, and the carrier mobility are similar. However, the electrostatic potential distribution and electric field profile of

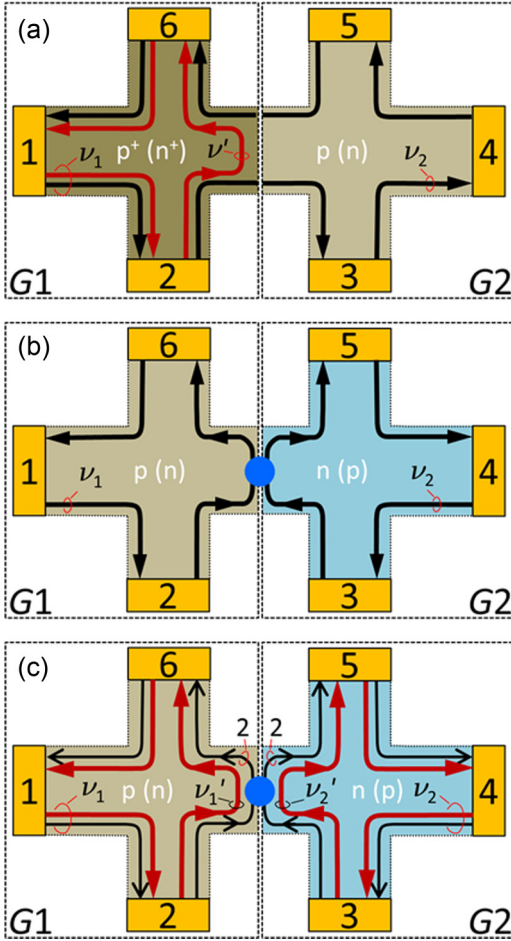


FIG. 3. (Color online) Schematic of edge-state transport model of longitudinal resistance  $R_{14,23}$  in the quantum Hall regime. The edge states in regions 1 and 2 are associated with filling factors  $\nu_1$  and  $\nu_2$ , respectively. (a) Model for junctions of the same polarity ( $pp+$  and  $nn+$ ). The number of edge states at the  $pnJ$  interface is  $\nu' = |\nu_1 - \nu_2|$ . Note that this model is independent of any assumption of equilibration of the edge states at the interface. (b) Model of full equilibration of edge states at the interface of a  $pnJ$ . (c) Model in which only the lowest Landau level edge states on opposite sides of the  $pnJ$  (marked by thin black lines) equilibrate. The energetically higher edge states (marked by thick red lines) are not equilibrated or interacting and  $\nu'_1 = |\nu_1 - 2|$  and  $\nu'_2 = |\nu_2 - 2|$ . Blue dots in (b) and (c) schematically indicate the region of edge-state equilibration and are not a detailed representation of carrier dynamics at the interface.

our device varies slowly as a function of position across the  $pnJ$  relative to that of [9]. Electrostatic simulations for our device geometry and that of [9] contrast the rate of change of the electrostatic potential across the  $pnJ$  (see Fig. S7 of [16]). The edge states at an electrostatically smooth junction are spatially further apart than those at a relatively abrupt junction. The larger spatial separation of Landau levels decreases the probability of edge states mixing. Thus we attribute the difference in equilibration in our device and that of [9] to the dramatic difference in the shape of the electrostatic junction.

To further confirm our lowest level equilibrated assumption, we explore the pseudo-Hall resistance  $R_{13,24}$  across the  $pnJ$  interface (Fig. 4). We chose the pseudo-Hall configuration to

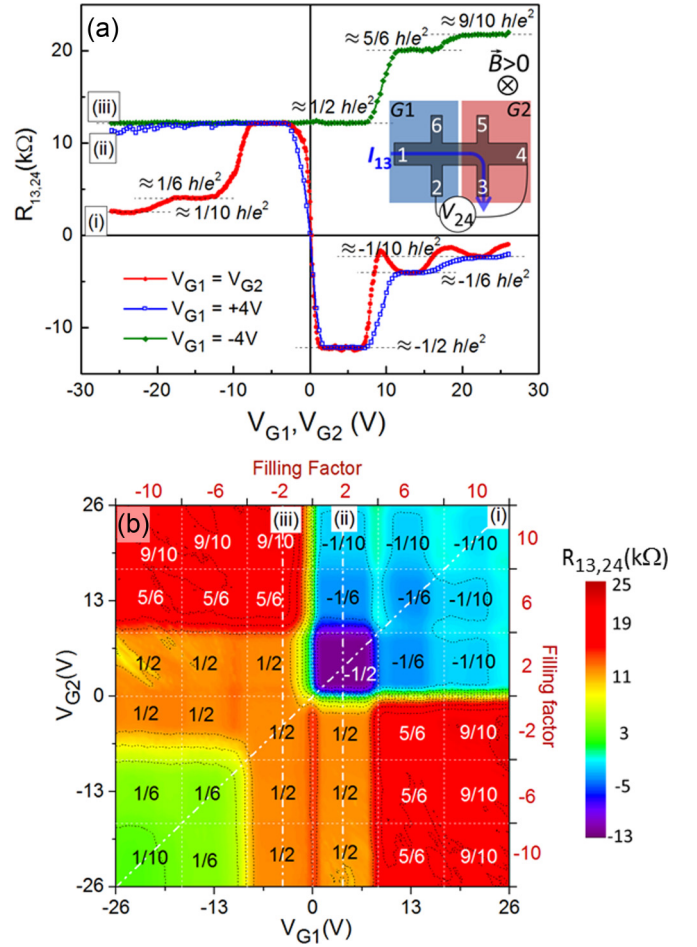


FIG. 4. (Color online) (a) Pseudo-Hall resistance  $R_{13,24}$  measured at  $T = 0.35$  K and  $B = +14$  T as a function of local gate voltages  $V_{G1}$  and  $V_{G2}$ ; (i)  $V_{G1} = V_{G2}$ , (ii)  $V_{G1} = +4$  V, and (iii)  $V_{G1} = -4$  V. Inset shows the corresponding measurement configuration. (b) 2D map of pseudo-Hall resistance  $R_{13,24}$  across the junction as a function of  $(V_{G1}, V_{G2})$  and filling factors  $(\nu_1, \nu_2)$ . Numbers inside the map are experimental plateau resistance values in units of  $h/e^2$  which are in full agreement with our predicted values. The dash-dotted lines correspond to (i), (ii), and (iii) curves in (a).

better probe transport across the junction instead of a pure Hall configuration ( $R_{14,26}$  or  $R_{14,35}$ ) which only probes the local region. In the case of uniform carrier concentration in the channel ( $V_{G1} = V_{G2}$ ) we observed typical quantum Hall resistance quantization sequences [Fig. 4(a), curve (i)]. In the bipolar ( $p-n$ ) regime, the pseudo-Hall resistance shows additional quantized plateaus, e.g.,  $9/10$  and  $5/6$  [Fig. 4(a), curve (iii)]. A complete map of  $R_{13,24}$  for independently swept  $V_{G1}$  and  $V_{G2}$  is shown in Fig. 4(b) with quantum plateaus located symmetrically about the  $V_{G1} = V_{G2}$  line.

Similar to the analysis of the longitudinal resistance map, the unipolar regions of Fig 4(b) ( $nnJ$  lower left and  $ppJ$  upper right) can be described within the Landauer-Büttiker edge-state transport model with no assumption on equilibration. Also similar to the longitudinal resistance map, the bipolar regions ( $pnJ$  or  $npJ$ ) can only be explained by the equilibration of only the lowest LL's edge states at the  $pnJ$ , calculated

to be

$$R_{14,23}(h/e^2) = \begin{cases} 1/(|\nu_1| - \nu'_1) + \nu'_2/|\nu_2|(|\nu_2| - \nu'_2), & p\text{-type region 1, } n\text{-type region 2,} \\ \nu'_1/|\nu_1|(|\nu_1| - \nu'_1) + 1/(|\nu_2| - \nu'_2), & n\text{-type region 1, } p\text{-type region 2.} \end{cases} \quad (3)$$

All predicted pseudo-Hall resistance plateaus up to filling factors  $\pm 10$  are experimentally resolved [Fig. 4(b)] fully supporting our model. To check the consistency of our measurements, we experimentally verified our device satisfies the Onsager reciprocity relation [20,24,25] for both the longitudinal  $R_{14,23}$  and pseudo-Hall  $R_{13,24}$  resistance maps:  $R_{kl,mn}(\mathbf{B}) = R_{mn,kl}(-\mathbf{B})$  [16].

Thus we have systematically measured both longitudinal and pseudo-Hall resistance maps across the  $pn$ J interface in

the quantum Hall regime covering a wide range of filling factors  $[|\nu_1, \nu_2| \leq 10]$ . We presented a model that assumes equilibration of only the lowest Landau level's edge states which describes the experimental data well over the whole range. In the future with controlled device engineering, one can take advantage of this fact to tailor a device for specific LL mixing selection for applications such as quantum Hall resistance standards with a wide and tunable range of resistance values other than  $h/2e^2$ .

- 
- [1] A. Rycerz, J. Tworzydło, and C. W. J. Beenakker, *Nat. Phys.* **3**, 172 (2007).
- [2] R. N. Sajjad and A. W. Ghosh, *Appl. Phys. Lett.* **99**, 123101 (2011).
- [3] A. F. Young and P. Kim, *Nat. Phys.* **5**, 222 (2009).
- [4] V. V. Cheianov, V. Fal'ko, and B. L. Altshuler, *Science* **315**, 1252 (2007).
- [5] M. Woszczyzna, M. Friedemann, T. Dziomba, T. Weimann, and F. J. Ahlers, *Appl. Phys. Lett.* **99**, 022112 (2011).
- [6] K. S. Novoselov, A. K. Geim, S. V. Morozov, D. Jiang, M. I. Katsnelson, I. V. Grigorieva, S. V. Dubonos, and A. A. Firsov, *Nature (London)* **438**, 197 (2005).
- [7] Y. Zhang, Y.-W. Tan, H. L. Stormer, and P. Kim, *Nature (London)* **438**, 201 (2005).
- [8] A. H. Castro Neto, F. Guinea, N. M. R. Peres, K. S. Novoselov, and A. K. Geim, *Rev. Mod. Phys.* **81**, 109 (2009).
- [9] J. R. Williams, L. DiCarlo, and C. M. Marcus, *Science* **317**, 638 (2007).
- [10] T. Lohmann, K. von Klitzing, and J. H. Smet, *Nano Lett.* **9**, 1973 (2009).
- [11] D. A. Abanin and L. S. Levitov, *Science* **317**, 641 (2007).
- [12] T. Low, *Phys. Rev. B* **80**, 205423 (2009).
- [13] J.-c. Chen, T. C. Au Yeung, and Q.-f. Sun, *Phys. Rev. B* **81**, 245417 (2010).
- [14] J. R. Williams and C. M. Marcus, *Phys. Rev. Lett.* **107**, 046602 (2011).
- [15] H. Schmidt, J. C. Rode, C. Belke, D. Smirnov, and R. J. Haug, *Phys. Rev. B* **88**, 075418 (2013).
- [16] See Supplemental Material at <http://link.aps.org/supplemental/10.1103/PhysRevB.92.241301> for additional experimental data and electrostatic simulations of the electric field and potential profile in our device.
- [17] S. Sutar, E. S. Comfort, J. Liu, T. Taniguchi, K. Watanabe, and J. U. Lee, *Nano Lett.* **12**, 4460 (2012).
- [18] C. R. Dean, A. F. Young, I. Meric, C. Lee, L. Wang, S. Sorgenfrei, K. Watanabe, T. Taniguchi, P. Kim, K. L. Shepard, and J. Hone, *Nat. Nanotechnol.* **5**, 722 (2010).
- [19]  $R_{ij,kl} = V_{kl}/I_{ij}$  current is driven between terminals  $i$  and  $j$ , and voltage is measure between  $k$  and  $l$ .
- [20] M. Büttiker, *Phys. Rev. Lett.* **57**, 1761 (1986).
- [21] D.-K. Ki, S.-G. Nam, H.-J. Lee, and B. Özyilmaz, *Phys. Rev. B* **81**, 033301 (2010).
- [22] B. W. Alphenaar, P. L. McEuen, R. G. Wheeler, and R. N. Sacks, *Phys. Rev. Lett.* **64**, 677 (1990).
- [23] C. A. Richter, R. G. Wheeler, and R. N. Sacks, *Surf. Sci.* **305**, 145 (1994).
- [24] L. Onsager, *Phys. Rev.* **37**, 405 (1931).
- [25] L. Onsager, *Phys. Rev.* **38**, 2265 (1931).